Macromolecules

Article

pubs.acs.org/Macromolecules

# Probing the Internal Morphology of Injectable Poly(oligoethylene glycol methacrylate) Hydrogels by Light and Small-Angle Neutron Scattering

Niels M. B. Smeets,[†] Emilia Bakaic,[†] Francis M. Yavitt,[†] Fei-Chi Yang,[‡] Maikel C. Rheinstädter,[‡] and Todd Hoare*,[†]

[†]Department of Chemical Engineering and [‡]Department of Physics and Astronomy, McMaster University, 1280 Main Street West, Hamilton, Ontario, Canada L8S 4L8

Supporting Information

**ABSTRACT:** While injectable, *in situ* gelling hydrogels have attracted increasing attention in the biomedical literature due to their minimally invasive administration potential, little is known about the internal morphology of these hydrogels and thus how to engineer precursor polymer compositions to achieve desired hydrogel properties. In this paper, the internal morphology of injectable *in situ* gelling hydrogels based on hydrazide and aldehyde-functionalized poly(oligoethylene glycol methacrylate) precursors with varying lower critical solution temperatures (LCSTs) is investigated using a combination of spectrophotometry, small-angle neutron scattering, and light scattering. If two precursor polymers with similar LCSTs are used to prepare the hydrogel, relatively homogeneous hydrogels are produced (analogous to conventional step-growth polymerized hydrogels); this result is observed provided that gelation is sufficiently slow for diffusional mixing to compensate for any incomplete mechanical mixing in the double-barrel syringe and the volume phase transition temperature (VPTT) of the hydrogel is sufficiently high that phase separation does not occur on the time scale of gelation. Hydrogels prepared from precursor polymers with different LCSTs (1 polymer/barrel) also retain transparency, although their internal morphology is significantly less homogeneous. However, if functionalized polymers with different LCSTs are mixed in each barrel (i.e., 2 polymers/barrel, such that a gelling pair of precursors with both low and high LCSTs is present), opaque hydrogels are produced that contain significant inhomogeneities that are enhanced as the temperature is increased; this suggests phase separation of the hydrogel into lower and higher LCST domains. Based on this work, the internal morphology of injectable hydrogels can be tuned by engineering the gelation time and the physical properties (i.e., miscibility) of the precursor polymers, insight that can be applied to improve the design of such hydrogels for biomedical applications.

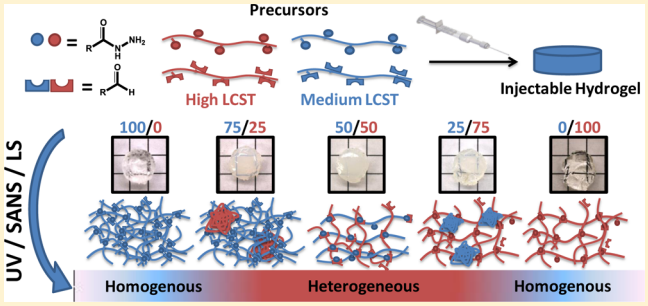


## INTRODUCTION

The success of hydrogels as soft synthetic materials for controlled release and cell scaffolding applications[1−4] can be attributed to high water content, controllable porosity, and mechanical and (if desired) compositional similarity of hydrogels to native tissues.[5] While various methods of gelation (e.g., physical, electrostatic, or chemical) exist for the fabrication of hydrogels, chemical (or covalent) cross-linking is generally preferred as it results in hydrogels with controllable stability under a variety of environmental conditions. The macroscopic properties of bulk hydrogels are largely governed by the homogeneity of the polymer network and can be significantly affected by cross-link inhomogeneities introduced during hydrogel formation. Depending on the target application, the presence of inhomogeneities in hydrogels may help (i.e., by providing domains of distinct compositions for loading and release applications) or hinder (i.e., by making hydrogels opaque or mechanically weaker) their ultimate use. A fundamental understanding of network homogeneity is therefore very important to fully understand the relationship between the hydrogel nanostructure and the macroscopic properties.[6]

Scattering methods, such as light scattering (LS) and small-angle neutron scattering (SANS), have been widely applied to probe the micro- and nanostructure of polymeric systems, including hydrogels.[7] In a hydrogel system, SANS allows for the determination of the mesh size ($\xi$) of the hydrogel network and characteristic size of inhomogeneities ($\Xi$) (or "blobs") formed as a result of nonideal cross-linking. Covalently cross-linked hydrogels fabricated via chain growth gelation (e.g., UV photopolymerization of vinyl monomers) generally give inhomogeneous hydrogels,[8] while chain growth polymerization

**Received:** June 7, 2014
**Revised:** August 4, 2014
**Published:** August 20, 2014

   dx.doi.org/10.1021/ma5011827 | *Macromolecules* 2014, 47, 6017−6027

Table 1. Composition of the Various POEGMA Hydrogels[a]

| | hydrazide barrel | | | aldehyde barrel | | |
|---|---|---|---|---|---|---|
| | $PO_0H_{30}$ [mg/mL] | $PO_{10}H_{30}$ [mg/mL] | $PO_{100}H_{30}$ [mg/mL] | $PO_0A_{30}$ [mg/mL] | $PO_{10}A_{30}$ [mg/mL] | $PO_{100}A_{30}$ [mg/mL] |
| $PO_0$ | 150.0 | | | 150.0 | | |
| $PO_{10}$ = PO(100/0) | | 150.0 | | | 150.0 | |
| PO(75/25) | | 112.5 | 37.5 | | 112.5 | 37.5 |
| PO(50/50) | | 75.0 | 75.0 | | 75.0 | 75.0 |
| PO(25/75) | | 37.5 | 112.5 | | 37.5 | 112.5 |
| $PO_{100}$ = PO(0/100) | | | 150.0 | | | 150.0 |
| $PO_{10}H_{30}$ + $PO_{100}A_{30}$ | | 150.0 | | | | 150.0 |
| $PO_{100}H_{30}$ + $PO_{10}A_{30}$ | | | 150.0 | | 150.0 | |

[a]All precursor solutions are prepared at 150 mg/mL in 10 mM PBS prior to mixing.

(e.g., mixing of complementary reactive polymeric precursors) has been demonstrated to generally yield more homogeneous hydrogels with fewer structural defects.[9] As a particularly relevant example of the latter, Matsunaga[6] demonstrated that a step growth hydrogel prepared from amine and succinimidyl ester functionalized 4-arm poly(ethylene glycol) (PEG) resulted in an extremely uniform hydrogel network without any detectable defects due to cross-linking inhomogeneities. Gelation in the case of injectable, *in situ* gelling hydrogels, in which a hydrogel is rapidly formed following *in situ* mixing of reactive polymers with complementary functional groups,[10] offers additional levels of complexity that may promote the formation of inhomogeneous domains in hydrogels. The rate and magnitude of polymer−polymer cross-linking in such systems are expected to be strongly dependent on not only the degree of functionalization of the pregel polymers but also the mixing and subsequent diffusion and/or phase separation of the reactive precursor polymers. The net effect of these competing processes has not been broadly investigated in the literature but is essential to understand to rationally engineer such *in situ* gelling hydrogels for biomedical applications.

We have recently reported the synthesis as well as physiochemical and biological properties of injectable poly(oligoethylene glycol methacrylate) (POEGMA) hydrogels.[11,12] Our approach is based on the rapid cross-linking of complementary reactive POEGMA precursors exploiting hydrazide−aldehyde chemistry.[13−20] On a macroscopic scale, the gelation kinetics, swelling, and mechanical properties of these POEGMA hydrogels depend strongly on the lower critical solution temperature (LCST) of the precursors,[11] which can be precisely tuned according to the statistical copolymerization of oligo(ethylene glycol) methacrylate (OEGMA) monomers with different ethylene oxide side chain lengths ($n$ = 2 and $n$ = 8, 9).[21,22] Substantial differences are observed in the physical properties of the hydrogels prepared with precursors with different LCST values despite the similarity in the theoretical cross-link density in each hydrogel, suggesting substantial differences in the structural homogeneity of the hydrogel network formed during gelation.

Herein, we aim to study in detail the nanostructure of injectable, thermoresponsive POEGMA hydrogels based on precursor polymers of different LCST values using SANS and LS. SANS and LS have been applied previously to characterize the structural changes in temperature responsive hydrogels based on (co)polymerization of *N*-isopropylacrylamide (PNIPAM)[23,24] (i.e., chain growth), indicating formation of microphase separated domains prior to the macroscopic phase transition.[23,24] However, to this point, there is no report investigating the microstructure of *in situ* gelling hydrogels from polymeric precursors or, more specifically, thermoresponsive *in situ* gelling hydrogels, despite the clinical relevance of such materials. We specifically aim to investigate the range of hydrogel morphologies that can be generated using precursor polymers with similar LCST values and/or divergent LCST values; in the latter case, the potential for phase separation on the time scale of gelation has the potential to yield particularly useful and novel morphologies of potential relevance for drug delivery or tissue engineering applications.

## EXPERIMENTAL SECTION

**Materials.** Di(ethylene glycol) methyl ether methacrylate (M(EO)$_2$MA, Sigma-Aldrich, 95%) and oligo(ethylene glycol) methyl ether methacrylate with an average number-average molecular weight of 475 g mol$^{-1}$ (OEGMA$_{475}$, Sigma-Aldrich, 95%) were purified by passing the monomers over a column of basic aluminum oxide (Sigma-Aldrich, type CG-20) to remove inhibitors. *N*-(2,2-Dimethoxyethyl)-methacrylamide (DMAEAm) was synthesized according to a previously reported procedure.[11] Acrylic acid (AA, Sigma-Aldrich, 99%), adipic acid dihydrazyde (ADH, Alfa Aesar, 98%), *N*′-ethyl-*N*-(3-(dimethylamino)propyl)carbodiimide (EDC, Carbosynth, Compton CA, commercial grade), thioglycolic acid (TGA, Sigma-Aldrich, 98%), and 2,2-azobisisobutryic acid dimethyl ester (AIBMe, Wako Chemicals, 98.5%) were used as received. For all experiments, Milli-Q grade distilled deionized water (DIW) was used.

**Synthesis of Hydrazide-Functionalized Precursors (POH).** Hydrazide-functionalized POEGMA precursors were synthesized as described previously.[11] Briefly, AIBMe, M(EO)$_2$MA, OEGMA$_{475}$, AA (0.36 g, 5.0 mmol), and TGA were dissolved in 1,4-dioxane. After purging for at least 30 min, the flask was sealed and submerged in a preheated oil bath at 75 °C for 4 h under magnetic stirring. The solvent was removed, and the polymer was modified with a large excess of adipic acid dihydrazide. The hydrazide functionalized polymer was purified by dialysis and lyophilized. The polymers were stored as 20% w/w solutions in PBS at 4 °C. The hydrazide-functionalized precursors are labeled as $PO_xH_y$, where $x$ denotes the mole fraction of OEGMA$_{475}$ among the OEGMA monomers used (the remainder being M(EO)$_2$MA) and $y$ denotes the overall mole fraction of AA (among all comonomers) in the synthesis recipe.

**Synthesis of Aldehyde-Functionalized Precursors (POA).** Aldehyde-functionalized POEGMA precursors were synthesized as described previously.[11] Briefly, AIBMe, M(EO)$_2$MA, OEGMA$_{475}$, DMEMAm, and TGA were dissolved in 1,4-dioxane. After purging for at least 30 min, the flask was sealed and submerged in a preheated oil bath at 75 °C for 4 h under magnetic stirring. The solvent was then removed, and the acetal was cleaved in 0.5 M hydrochloric acid to generate the aldehyde group. The resulting aldehyde functionalized polymer was purified by dialysis and lyophilized. The polymers were stored as 20% w/w solutions in PBS at 4 °C. The aldehyde-functionalized precursors are labeled as $PO_xA_y$, where $x$ denotes the mole fraction of OEGMA$_{475}$ among the OEGMA monomers used (the remainder being M(EO)$_2$MA) and $y$ denotes the overall mole fraction of DMEMAm (among all comonomers) in the synthesis recipe.


dx.doi.org/10.1021/ma5011827 | Macromolecules 2014, 47, 6017−6027

**Chemical Characterization.** Aqueous size exclusion chromatography (SEC) was performed using a Waters 515 HPLC pump, a Waters 717 Plus autosampler, three Ultrahydrogel columns (30 cm × 7.8 mm i.d.; exclusion limits: 0−3, 0−50, and 2−300 kDa), and a Waters 2414 refractive index detector. A mobile phase consisting of 0.3 M sodium nitrate and 0.05 M phosphate buffer (pH 7) at a flow rate of 0.8 mL/min was used for all polymers analyzed, and the system was calibrated with narrow-dispersed poly(ethylene glycol) standards ranging from 106 to 584 × $10^3$ g/mol (Waters). $^1$H NMR was performed using a Bruker AVANCE 600 MHz spectrometer and deuterated chloroform as the solvent. The acrylic acid content of the polymers was determined with conductometric titration (ManTech Associates), using 50 mg of polymer dissolved in 50 mL of 1 mM NaCl as the analysis sample and 0.1 M NaOH as the titrant. A Variant Cary Bio 100 UV−vis spectrophotometer was used to measure the LCST (defined as 95% transmittance) of the polymer precursor chains. The polymers were dissolved at a concentration of 1 mg/mL in PBS (pH = 7.4), and the absorbance of the polymer solution was recorded at 500 nm at every 0.5 °C over a temperature range of 10−80 °C, with the temperature ramped at a rate of 1 °C/min.

**Hydrogel Preparation.** Hydrogels were prepared by coextruding one or more hydrazide-functionalized precursor(s) (among $PO_0H_{30}$, $PO_{10}H_{30}$, and $PO_{100}H_{30}$) with one or more aldehyde-functionalized precursor(s) (among $PO_0A_{30}$, $PO_{10}A_{30}$, and $PO_{100}A_{30}$) using a double-barrel syringe (Medmix). Table 1 provides a complete summary of the hydrogel recipes evaluated.

Hydrogels were prepared by coextruding (i) precursors of similar LCST ($PO_0$ = $PO_0H_{30}$ + $PO_0A_{30}$; $PO_{10}$ = $PO_{10}H_{30}$ + $PO_{10}A_{30}$; $PO_{100}$ = $PO_{100}H_{30}$ + $PO_{100}A_{30}$), (ii) precursors with different LCSTs in each barrel (i.e., $PO_{10}H_{30}$ + $PO_{100}A_{30}$ and $PO_{100}H_{30}$ + $PO_{10}A_{30}$), or (iii) mixed precursors of different LCSTs in different weight ratios (PO(75/25), PO(50/50), and PO(25/75)). This latter group of hydrogels was prepared in a similar manner as the $PO_{10}$ and $PO_{100}$ hydrogels; however, precursor solutions were prepared by mixing both high LCST and low LCST precursor polymers in both the hydrazide ($PO_{10}H_{30}$ and $PO_{100}H_{30}$) and aldehyde ($PO_{10}A_{30}$ and $PO_{100}A_{30}$) barrels of the double-barrel syringe at a total concentration of 150 mg/mL in the mass ratios indicated by the hydrogel sample codes. As such, each mixed precursor hydrogel is prepared with four precursor polymers (2 hydrazide-functionalized and 2 aldehyde-functionalized) while all other hydrogels studied are prepared by mixing only two precursor polymers (1 hydrazide-functionalized and 1 aldehyde-functionalized).

**Gelation Kinetics.** The transmittance of the hydrogels was tracked during the gelation process using a Cary 300 UV−vis spectophotometer with the Kinetics Software (version 3.0). The polymer precursor solutions (500 μL at 150 mg/mL) were coextruded into a polystyrene cuvette, and the absorbance was tracked at a wavelength of 500 nm with an average sample time of 0.1 s and cycle time of 0.25 min. All experiments were performed with the Peltier unit set at 37 °C to maintain constant temperature mimicking physiological injection.

**Phase Transition of the Hydrogels.** The volume phase transition temperature of the hydrogels (300 μL) was determined gravimetrically. Hydrogel disks were prepared by extruding the reactive polymer precursors through the double-barrel syringe into cylindrical silicone rubber molds (diameter = 7 mm, volume = 300 μL). Hydrogels were placed inside scintillation vials filled with 12 mL of 10 mM PBS and submerged into a thermostated water bath. After a 12 h incubation period to ensure complete gelation, the hydrogels were gently dried using a Kimwipe to remove nonabsorbed PBS and weighed. A fresh aliquot of PBS was then added, the temperature of the water bath increased by 5 °C, and the process was repeated. The mass loss of the hydrogels was calculated by comparing the mass of the hydrogel at any given temperature to the initial mass of the same hydrogel, as measured at 22.5 °C (room temperature). All experiments were performed in triplicate, with reported error bars representing the standard error of the repeat measurements.

**Small-Angle Neutron Scattering (SANS).** SANS experiments were conducted using the 30 m SANS NG3 at the NIST Center for Neutron Research (NCNR, Gaithersburg, MD). The sample-to-detector distances were 1, 4, and 13 m (with and without lenses), using neutron wavelengths of 6 Å for the first three configurations and 8.4 Å for the 13 m lensed distance. The wavelength spread was 13%. All precursor polymers for SANS experiments were dissolved at a total concentration of 150 mg/mL in 10 mM phosphate buffered $D_2O$ to facilitate neutron scattering contrast. Hydrogels were subsequently extruded from a double-barrel syringe into a demountable 4.32 × 3.49 × 2.16 $cm^3$ sample cell (titanium body and quartz windows) provided by NCNR and set to an internal gap thickness of 1 mm, requiring ∼300 μL of hydrogel. Polymers extruded into sample cells were left to completely gel for 12 h before measurements were performed. The low $q$ range data were acquired by counting for 15 min using the 13 m detection distance followed by 20 min using the 13 m distance with lens. The medium $q$ range was collected using a 4 m detection distance counting for 5 min. The high $q$ range was collected using a 1 m detection distance counting for 2 min. The four ranges of data collected were then merged using the DAVE on-site data reduction tool.

**Light Scattering (LS).** The light scattering experiment was conducted using a 5 mW laser diode operating at a wavelength of 532 ± 10 nm. Scattered light was detected using a ThorLabs DET10A Si biased detector sensitive to wavelengths from 200 to 1100 nm. Hydrogel precursors dissolved at 150 mg/mL in 10 mM PBS were extruded directly into standard 1 cm × 1 cm quartz cuvettes to a total volume of 1.2 mL, yielding a typical beam size of 1.5 mm, sample thickness of 10 mm, and sample height of 2 mm. The detector was mounted on a motor-controlled Huber diffractometer with a laser-to-sample distance of 40 cm and sample-to-detector distance of 35 cm. Motor positions were controlled to precision of at least 0.01°. A detector angle ($2\theta$) range of −60° to 60° was scanned, with the scattered light intensity recorded. This angular range was determined in test experiments to cover the experimental features, as will be shown below. A typical experimental run required approximately 160 min to collect data over the full angular range.

## THEORY

The scattering intensity ($I(q)$) homogeneity of hydrogel networks has been described by eq 1, a summation of dynamic (or fluid-like) fluctuations represented by an Ornstein−Zernike function ($I_{OZ}(q)$, eq 2)[25] and static (or solid-like) fluctuations represented by a squared Lorenzian function ($I_{SL}(q)$, eq 3).[7,24]

$$I(q) = \frac{\Delta\rho^2 RT\phi^2}{N_A M_{OS}}\left[\frac{I_{OZ}(0)}{1+\xi^2 q^2} + \frac{I_{SL}(0)}{(1+\Xi^2 q^2)^2}\right] \quad (1)$$

$$G(q) \sim I_{OZ}(q) = \frac{I_{OZ}(0)}{1+\xi^2 q^2} \quad \text{(Ornstein−Zernicke)} \quad (2)$$

$$C(q) \sim I_{SL}(q) = \frac{I_{SL}(0)}{(1+\Xi^2 q^2)^2} \quad \text{(squared Lorentzian)} \quad (3)$$

In eqs 1−3, $q$ is the scattering vector, $\Delta\rho^2$ the scattering length density difference squared, $\varphi$ the volume fraction of the solute, $N_A$ Avogadro's number, $R$ the universal gas constant, $T$ the temperature, $M_{OS}$ the osmotic modulus, $\xi$ the correlation length, and $\Xi$ the characteristic size of inhomogeneities. The key parameters yielding insight into the hydrogel morphology are the $\xi$, the correlation length (or mesh size) of the network, and $\Xi$, the characteristic size of the inhomogeneities (or "blobs") formed as a result of cross-linking. The latter can also be expressed in terms of a radius of gyration of the polymer rich/poor domains ($R_g = 3^{0.5}\Xi$). In the case of an ideal hydrogel network, $I(q)$ can be described by the dynamic fluctuations only, as was demonstrated experimentally for the 4-arm tetra-poly(ethylene glycol) hydrogel network discussed in the


dx.doi.org/10.1021/ma5011827 | Macromolecules 2014, 47, 6017−6027

Table 2. Chemical Characterization of Synthesized POEGMA Polymer Precursors

| | $M(EO)_2MA^a$ [mol %] | $OEGMA_{475}{}^a$ [mol %] | functional monomer [mol %] | $M_n{}^c$ [$10^3$ g mol$^{-1}$] | $Đ^c$ | functional groups [no./chain] | $LCST^d$ [°C] |
|---|---|---|---|---|---|---|---|
| $PO_0H_{30}$ | 77.1 | 0.0 | 22.9[b] | 16.2 | 2.41 | 24 | 51.0 |
| $PO_{10}H_{30}$ | 72.5 | 5.9 | 21.6[b] | 17.0 | 2.08 | 22 | 63.0 |
| $PO_{100}H_{30}$ | 0.00 | 72.8 | 27.2[b] | 19.4 | 2.35 | 16 | >80 |
| $PO_0A_{30}$ | 80.6 | 0.0 | 19.4[a] | 16.9 | 2.49 | 17 | 40.1 |
| $PO_{10}A_{30}$ | 70.4 | 5.7 | 23.9[a] | 13.0 | 2.03 | 19 | 53.5 |
| $PO_{100}A_{30}$ | 0.00 | 71.9 | 28.1[a] | 18.3 | 2.43 | 16 | >80 |

[a]Determined by $^1$H NMR. [b]Determined from conductometric titration. [c]Measured using aqueous SEC using an acetate buffer. [d]Determined at 95% transmittance at a concentration of 1 mg/mL in PBS. Synthesis data reproduced from ref 11.

Introduction.[6] However, in most cases (and particularly in the case of the *in situ* gelling hydrogels prepared from precursors with different phase transitions described herein), chemical cross-linking is nonideal, and resulting inhomogeneities are observed as static fluctuations.

## RESULTS

**Synthesis of the Reactive Poly(oligoethylene glycol methacrylate) Precursors.** Three sets of $PO_xH_y$ and $PO_xA_y$ precursors were synthesized with varying ratios of $M(EO)_2MA$ and $OEGMA_{475}$ ($x$ = 0, 10, and 100 mol %, resulting in precursor polymers with various lower critical solution temperatures), similar degrees of hydrazide and aldehyde functionalization ($y$ = 30 mol %), and similar number-average molecular weights ($M_n$). Given that the functional group density and the molecular weight of all polymers generated in this work are similar, each precursor has a similar average number of functional groups per chain (19 ± 3, Table 2) but differs in terms of lower critical solution temperature (LCST).

**Preparation of Poly(oligoethylene glycol methacrylate) Hydrogels.** Single precursor POEGMA hydrogels were prepared such that (1) one $PO_xH_{30}$ and $PO_xA_{30}$ precursor are used and both precursors are similar in terms of their $M(EO)_2MA$:$OEGMA_{475}$ composition ($x$ = 0, 10, or 100 mol %) and (2) the $PO_xH_{30}$ and $PO_xA_{30}$ precursors are dissolved at equal concentrations (150 mg/mL in each barrel); by extension, based on the similar functional group densities among all precursors as shown in Table 2, a nearly 1:1 ratio of aldehyde:hydrazide functional groups is present within each hydrogel composition tested. The resulting hydrogels are labeled according to the corresponding mole fraction of $OEGMA_{475}$ used to prepare the precursors ($x$): $PO_0$ = $PO_0H_{30}$ + $PO_0A_{30}$, $PO_{10}$ = $PO_{10}H_{30}$ + $PO_{10}A_{30}$, and $PO_{100}$ = $PO_{100}H_{30}$ + $PO_{100}A_{30}$ (Table 1). As a result of the difference in OEGMA monomer composition ($x$), the thermoresponsive properties of the $PO_0$, $PO_{10}$, and $PO_{100}$ hydrogels differ substantially; the $PO_{10}$ hydrogel displayed a volume phase transition temperature (VPTT) at ~32 °C, compared to ~22 °C for $PO_0$ and >90 °C for $PO_{100}$.[11] The optical appearance of the $PO_0$, $PO_{10}$, and $PO_{100}$ hydrogels below and above their VPTT is shown in Figure 1A–F (note that given the high VPTT of the $PO_{100}$ hydrogels, both temperatures tested in Figure 1C,F were below the VPTT of those hydrogels).

The $PO_{100}$ hydrogel remains transparent and swollen upon heating from 22 to 37 °C, as anticipated for high transition temperature hydrogel. The $PO_{10}$ hydrogel undergoes a volume phase transition at ~32 °C, transitioning from transparent below the VPTT (Figure 1B) to translucent above the VPTT (Figure 1E). In contrast, the $PO_0$ hydrogel appears opaque both below (Figure 1A) and above (Figure 1D) the VPTT,

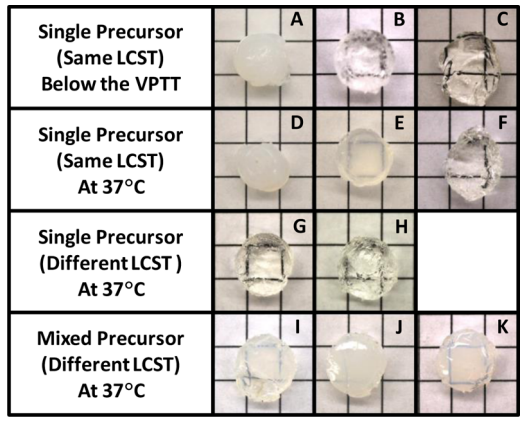


**Figure 1.** Optical appearance of the various POEGMA hydrogels prepared for the SANS study. Images of the single precursor $PO_0$ (A), $PO_{10}$ (B), and $PO_{100}$ (C) hydrogels below their VPTT (5 °C for $PO_0$ and 22 °C for $PO_{10}$ and $PO_{100}$). All other images were recorded at 37 °C: $PO_0$ (D), $PO_{10}$ (E), $PO_{100}$ (F), $PO_{100}H_{30}$ + $PO_{10}A_{30}$ (G), $PO_{10}H_{30}$ + $PO_{100}A_{30}$ (H), PO(25/75) (I), PO(50/50) (J), and PO(75/25) (K). All precursor solutions were filtered with a 0.45 μm PFTE filter to remove dust and other impurities that might otherwise impart the optical transparency of the resulting hydrogel.

suggesting that the opaque appearance of the $PO_0$ hydrogels is not solely a result of the phase transition behavior of the hydrogel (i.e., formation of internal inhomogeneities on the length scale of visible light is likely). Despite the similarity in the theoretical cross-link density ($y$ = 30 mol %) between the different gels, significant differences in the macroscopic gelation time as well as the mechanical properties exist between the $PO_0$, $PO_{10}$, and $PO_{100}$ hydrogels.[11] The macroscopic gelation time ranges from <5 s for $PO_0$ to <10 s for $PO_{10}$ to 1200 s for $PO_{100}$, while the elastic storage modulus ($G'$) and calculated cross-link density ($\nu$) of $PO_0$ are roughly 1 order of magnitude higher than those of $PO_{100}$.[11] We postulated that these property differences may originate from the differing availabilities of the aldehyde and hydrazide functional groups for cross-linking reactions due to steric hindrance by the bulky ethylene oxide ($n$ = 8–9) side chains of $OEGMA_{475}$.[11]

Mixed precursor hydrogels were also produced, exploiting the facile modularity of our approach to injectable hydrogel formation[13,14] in that multiple precursors with the same functionalization (hydrazide or aldehyde) can be mixed at varying ratios to form a hydrogel that exhibits the combined properties of the precursor mixture following simple coextrusion.[26,27] Mixed precursor POEGMA hydrogels were prepared by mixing $PO_{10}H_{30}$, $PO_{100}H_{30}$, $PO_{10}A_{30}$, and $PO_{100}A_{30}$ precursors such that (1) an equal weight ratio of $x$ = 10 and $x$ = 100 precursors is added to both the hydrazide and


dx.doi.org/10.1021/ma5011827 | Macromolecules 2014, 47, 6017–6027

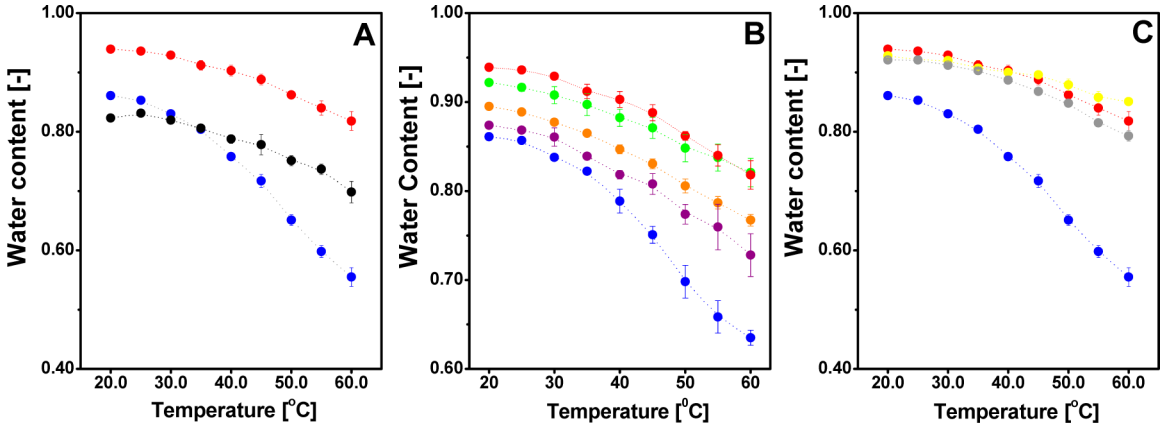


**Figure 2.** Equilibrium water content of the mixed precursor POEGMA hydrogels as a function of the temperature: $PO_0$ (black), $PO_{10}$ = PO(100/0) (blue), PO(75/25) (green), PO(50/50) (orange), PO(25/75) (purple), $PO_{100}$ (red), $PO_{10}H_{30}$ + $PO_{100}A_{30}$ (yellow), and $PO_{100}H_{30}$ + $PO_{10}A_{30}$ (gray). Data in (A) reproduced from ref 11.

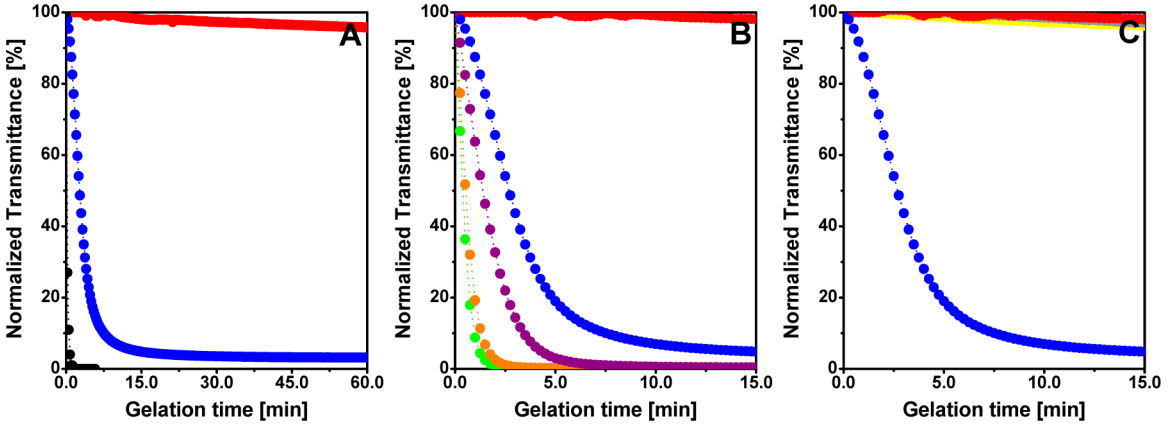


**Figure 3.** Evolution of the normalized transmittance during gelation of the single precursor (same LCST) (A), single precursor (different LCST) (B), and mixed precursor and (C) POEGMA hydrogels as measured by UV−vis spectrophotometry at 37 °C. $PO_0$ (black), $PO_{10}$ = PO(100/0) (blue), PO(75/25) (green), PO(50/50) (orange), PO(25/75) (purple), $PO_{100}$ (red), $PO_{10}H_{30}$ + $PO_{100}A_{30}$ (yellow), and $PO_{100}H_{30}$ + $PO_{10}A_{30}$ (gray).

aldehyde barrels of the double-barrel syringe and (2) the aldehyde ($PO_xA_{30}$) and the complementary hydrazide ($PO_xH_{30}$) precursor solutions are both prepared at a total concentration of 150 mg/mL, such that (based on the similar functional group densities among all precursors as shown in Table 2) a ∼1:1 ratio of aldehyde:hydrazide functional groups is present within each hydrogel composition tested (Table 1). Note that in this case gelation can occur without significant cross-reaction of $PO_{10}$ and $PO_{100}$ precursors, as both hydrazide and aldehyde-functionalized prepolymers of each LCST are always present. Five hydrogels were prepared by mixing the precursors with $x$ = 10 and $x$ = 100 mol % in 100/0, 75/25, 50/50, 25/75, and 0/100 weight ratios (for example, the 25/75 wt % hydrogel was prepared by mixing 25% w/w $PO_{10}H_{30}$ with 75% w/w $PO_{100}H_{30}$ in the hydrazide barrel and 25% w/w $PO_{10}A_{30}$ and 75% w/w $PO_{100}A_{30}$ in the aldehyde barrel and coextruding the mixture through the mixing channel). The macroscopic gelation time of these hydrogels increases exponentially with increasing $PO_{100}H_{30}$ and $PO_{100}A_{30}$ content of the precursors from <10 s for PO(75/25) to 20 s for PO(50/50) and 230 s for PO(25/75).

Whereas the single-component $PO_{10}$ and $PO_{100}$ hydrogels are both transparent below the VPTT (Figure 1B,C), the mixed PO(75/25), PO(50/50), and PO(25/75) hydrogels all appear translucent/opaque (Figure 1I−K). The VPTT of these mixed hydrogels was measured gravimetrically (Figure 2) and resembles that of the $PO_{100}$ hydrogels, as all hydrogels show a gradual decrease in the water content and no discrete volume phase transition as the temperature increases from 20 to 60 °C (although the absolute water content of the hydrogels scales directly with the fraction of the low LCST precursor included in the hydrogel, Figure 2). Even the PO(75/25) hydrogel, which consists of 75% w/w low LCST precursor, exhibits a broad and nondiscrete phase transition temperature, suggesting that introducing even small fractions of high LCST precursors effectively eliminates the discrete VPTT observed for the $PO_{10}$ hydrogel. The absence of a discrete VPTT up to 60 °C coupled with the observed opacity of the mixed precursor POEGMA hydrogels suggests that these hydrogels are less homogeneous than the corresponding single precursor POEGMA hydrogels.

For comparison, two additional single precursor hydrogels were prepared by coextruding one hydrazide-functionalized and one aldehyde-functionalized POEGMA precursor of different LCST. These hydrogels are prepared such that (1) one $PO_xH_{30}$ and $PO_xA_{30}$ precursor respectively are used of different $M(EO)_2MA$:$OEGMA_{475}$ composition ($x$ = 10 or 100 mol %) and (2) the $PO_xH_{30}$ and $PO_xA_{30}$ precursors are dissolved at equal concentrations (150 mg/mL in each barrel); as before,


dx.doi.org/10.1021/ma5011827 | Macromolecules 2014, 47, 6017−6027

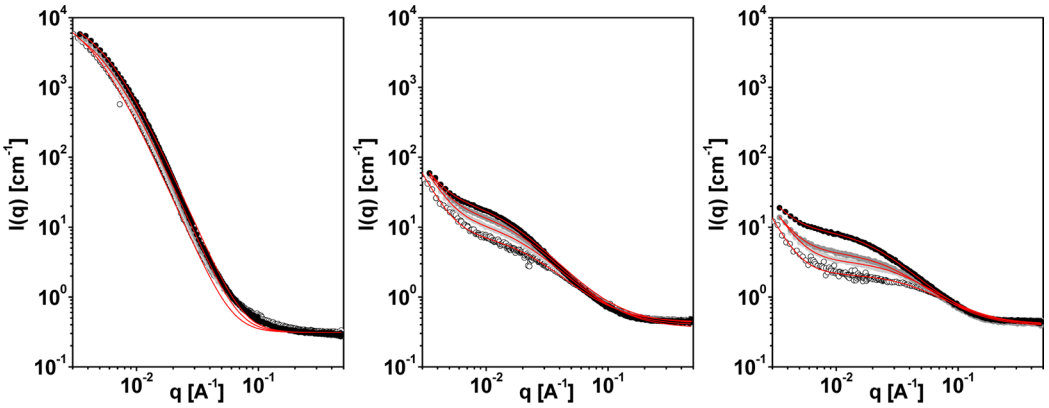


**Figure 4.** Scattering intensity of the $PO_0$ (A), $PO_{10}$ (B), and $PO_{100}$ (C) hydrogels as a function of temperature: (open circle) 22 °C, (light gray circle) 32 °C, (dark gray circle) 37 °C, and (black circle) 45 °C. The Ornstein−Zernike (OZ)−squared Lorentzian (SL) fits of the scattering intensities are shown as the red solid lines.

based on the similar functional group densities among all precursors as shown in Table 2, a reactive functional group ratio of ∼1:1 is achieved. Contrary to the mixed precursor hydrogels that also consist of precursors of different LCSTs, the $PO_{100}H_{30}$ + $PO_{10}A_{30}$ (Figure 1G) and $PO_{10}H_{30}$ + $PO_{100}A_{30}$ (Figure 1H) hydrogels are transparent. Gelation of these hydrogels occurs after 20 s for $PO_{10}H_{30}$ + $PO_{100}A_{30}$ and 230 s for $PO_{100}H_{30}$ + $PO_{10}A_{30}$, a similar time scale range to the mixed precursor hydrogels that were opaque. Based on these observations, if gelation is forced between precursors with different LCSTs (single precursor/different LCST hydrogels), the resulting gels are transparent; if gelation can still occur without cross-reaction of precursors with different LCSTs (mixed precursor hydrogels), the hydrogels are translucent or opaque.

**Kinetics of Structure Development.** The optical transmittance during gelation of the single and mixed precursor POEGMA hydrogels was measured by coextruding the reactive precursors (at 22 °C) directly into a UV−vis cuvette incubated at 37 °C (Figure 3A−C and Supporting Information Figure S1).

Although the LCSTs of both $PO_0$ precursors are >37 °C ($PO_0H_{30}$ = 51.0 °C and $PO_0A_{30}$ = 40.1 °C, Table 2), $PO_0$ gels within seconds and, upon cross-linking, the VPTT quickly drops below 37 °C and the $PO_0$ hydrogel adopts a milky white appearance with 0% transmittance (Figure 3A). In comparison, the normalized transmittance of the $PO_{10}$ hydrogel decreases more slowly after coextrusion into the UV cuvette, reaching nearly 0% only after ∼15 min (Figure 3A). Interestingly, while opacity changes are observed over several minutes, macroscopic gelation occurs much more quickly (<10 s); this result suggests that the observed decrease in transmittance has to be primarily accounted to a volume phase transition that occurs as the cold hydrogel formed quickly after extrusion (22 °C) is heated to 37 °C in the cuvette; this is analogous to the opacity change observed for the $PO_{10}$ hydrogel in Figure 1B,E upon heating. However, the evolution of inhomogeneities at higher cross-link densities cannot be dismissed as a possible mechanism for this higher opacity. The $PO_{100}$ hydrogel shows virtually no change in normalized transmittance up to 1 h postextrusion (i.e., past the point that bulk gelation has occurred), since the VPTT of the hydrogel at any degree of cross-linking achieved remains well above 37 °C.

Comparable to the $PO_{10}$ hydrogel, the mixed precursor PO(75/25), PO(50/50), and PO(25/75) hydrogels show a decrease in the normalized transmittance over the initial 10 min of the experiment (Figure 3B). However, the evolution of transmittance changes faster for the mixed precursor hydrogels than for either constituent single precursor hydrogel; in particular, the PO(75/25) and PO(50/50) hydrogels turn completely opaque within 1 min, on a time scale similar to macroscopic gelation of these samples, while single component gels fabricated from $PO_{10}$ or $PO_{100}$ precursors took much longer to turn opaque (∼15 min for $PO_{10}$) or did not turn opaque whatsoever ($PO_{100}$). This result seems to suggest that opaque appearance of the mixed precursor hydrogels is not caused by a phase change (Figure 3) but rather is a consequence of phase separation during the time scale of gelation. In comparison, single precursor hydrogels prepared by coextruding one $PO_{10}$ precursor and one $PO_{100}$ precursor (i.e., $PO_{10}H_{30}$ + $PO_{100}A_{30}$ and $PO_{100}H_{30}$ + $PO_{10}A_{30}$) were both highly transparent (Figure 1G,H) and demonstrated no significant measured decrease in the normalized transmittance over time (Figure 3C), consistent with the physical appearance of the hydrogels in Figure 1.

**SANS of Single Precursor POEGMA Hydrogels.** The neutron scattering intensity, $I(q)$, as a function of the scattering vector ($q$) was measured for $PO_0$, $PO_{10}$, and $PO_{100}$ at four different temperatures navigated around the VPTT of the $PO_{10}$ hydrogel (Figure 4A−C). The neutron scattering intensity curve for $PO_0$ shows a single-exponential decay, whereas the neutron scattering intensity curves of $PO_{10}$ and $PO_{100}$ show two decays. Furthermore, the $I(q)$ of the $PO_0$ hydrogel at low $q$ (i.e., $q < 10^{-2}$ Å$^{-1}$) is roughly 2 orders of magnitude higher than the $I(q)$s of the $PO_{10}$ and $PO_{100}$ hydrogels. These observations suggest that the $PO_{10}$ and the $PO_{100}$ hydrogels are more homogeneous than the $PO_0$ hydrogel on the length scale investigated here (roughly 1−200 nm). It should also be noted that the cross-link density of $PO_0$ was observed to be approximately 1 order of magnitude higher than that of $PO_{100}$,[11] which would also contribute to the higher scattering intensity observed for $PO_0$ even in the absence of heterogeneities. The scattering intensity curves were successfully fitted using eq 1, with generally good fits obtained ($R^2$ > 0.99). The fit parameters describing the network characteristics ($\xi$ and $\Xi$) are plotted as a function of the temperature in Figure 5A,B.

The neutron scattering intensity curves obtained for $PO_0$ show a single-exponential decay (Figure 4A) and could be successfully described only accounting for the contribution of


dx.doi.org/10.1021/ma5011827 | Macromolecules 2014, 47, 6017−6027

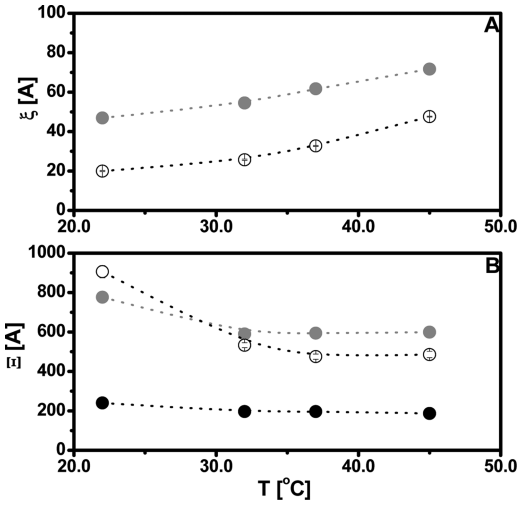


**Figure 5.** Correlation length of the hydrogel network $\xi$ (A) and the characteristic size of inhomogeneities $\Xi$ (B) for the single precursor $PO_0$ (black circle), $PO_{10}$ (gray circle), and $PO_{100}$ (open circle) hydrogels as a function of the measurement temperature from mathematical fits of the neutron scattering intensity curves using eq 1. Note: the correlation length for $PO_0$ hydrogel could not be determined due to the heterogeneity of the hydrogel (i.e., no fluid contribution was relevant).

the static fluctuations (Supporting Information Figure S2). Upon coextrusion the $PO_0H_{30}$ and $PO_0A_{30}$ precursors, macrogelation occurs virtually instantaneously and a heterogeneous hydrogel network is formed. We hypothesize this heterogeneity is derived from the incomplete mechanical mixing provided by the static mixer of the double barrel syringe, as gelation happens too fast and at too great an extent (owing to the highest cross-link density measured for this gel) for diffusional mixing to significantly change the mass distribution of the reactive polymers within the hydrogel phase. Existing concentration fluctuations (e.g., due to chain entanglement in solution) are frozen into the hydrogel network structure, as chain mobility is restricted by the fast cross-link formation. Consequently, no ordered hydrogel network is constructed, and no defined mesh size can be determined for this hydrogel. Rather, the SANS experiments suggest that this hydrogel network consists of a densely cross-linked chaotic network of static inhomogeneities. The scattering intensity curves show no dependence on the measurement temperature (Figure 4A), and consequently, no temperature dependence of $\Xi$ was observed (Figure 5B). This is consistent with the nearly constant water content measured as a function of the temperature in the gravimetric swelling experiments shown in Figure 2A. As the VPTT of the $PO_0$ hydrogel is approximately 22 °C, it can be expected that the hydrogel is in a dehydrated and collapsed state even at the lowest measurement temperature of 22 °C.

The $PO_{10}$ and $PO_{100}$ hydrogels (Figure 4B,C) are more homogeneous, and the $I(q)$ curves were successfully described only by considering a summation of dynamic and static fluctuations (Supporting Information Figures S3 and S4). The difference in network homogeneity between the $PO_{10}$ and the $PO_0$ hydrogel is striking considering that macroscopic gelation of the $PO_{10}H_{30}$ and $PO_{10}A_{30}$ precursors (<5 s) occurs only marginally slower than for the $PO_0H_{30}$ and $PO_0A_{30}$ precursors. The somewhat slower gelation kinetics and lower ultimate cross-link density achieved for $PO_{10}$ relative to $PO_0$ (~3-fold lower cross-link density based on mechanics calculations)[11] better facilitates spatial reorientation of the polymer chains during cross-linking and consequently locks the precursors in a more homogeneous hydrogel network. Homogeneity is also promoted by the lack of an ongoing phase transition as a function of cross-linking (i.e., the hydrogel phase transition temperature still lies above room temperature even after cross-link formation).

Slowing the gelation kinetics even more (macrogelation for the $PO_{100}H_{30}$ and $PO_{100}A_{30}$ precursors occurs in approximately 1200 s) reduces $I(q)$ to a lesser extent but does result in a significantly more homogeneous hydrogel network. Furthermore, parallel to the gelation kinetics, the cross-link density also decreases[11] which also attributes to lower scattering and the production of a more homogeneous hydrogel.[28,29] In addition, for both $PO_{10}$ and $PO_{100}$, unlike for $PO_0$, temperature has a clear impact on the hydrogel mesh size ($\xi$) (positive correlation) and the size of inhomogeneities ($\Xi$) (negative correlation) observed (Figure 5A,B).

**SANS of Mixed Precursor POEGMA Hydrogels.** The neutron scattering intensity of the mixed precursor PO(75/25),

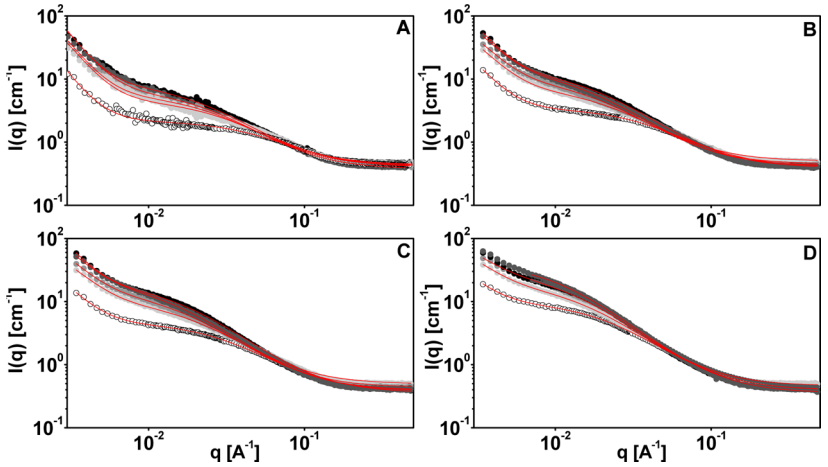


**Figure 6.** Scattering intensity of the mixed POEGMA hydrogels as 22 (A), 32 (B), 37 (C), and 45 °C (D) as a function of hydrogel composition: (open circle) PO(0/100) (= $PO_{100}$), (light gray circle) PO(25/75), (gray circle) PO(50/50), (dark gray circle) PO(75/25), and (black circle) PO(100/0) (= $PO_{10}$). The Ornstein–Zernike (OZ)–squared Lorentzian (SL) fits of the scattering intensities are shown as the red solid lines.


dx.doi.org/10.1021/ma5011827 | Macromolecules 2014, 47, 6017–6027

PO(50/50), and PO(25/75) hydrogels was measured for each hydrogel at four different temperatures navigated around the VPTT of the PO(100/0) (= $PO_{10}$) hydrogel and compared to the single component PO(100/0) (= $PO_{10}$) and PO(0/100) (= $PO_{100}$) hydrogels (Figure 6A–D). Independent of the measurement temperature, the scattering intensity at low $q$ ($<10^{-1}$ Å) increases with increasing weight fraction of the $PO_{10}$ precursors. There is only a marginal increase in the scattering intensity as the measurement temperature is increased from 22 to 45 °C for all the mixed precursor hydrogels tested (Figure 6). This suggest that none of these heterogeneous precursor hydrogels undergo a bulk phase transition up to 45 °C, in line with the SANS measurements shown in Figure 4B,C for the $PO_{10}$ and $PO_{100}$ hydrogels and the volumetric deswelling data shown in Figure 2. The scattering intensity curves of all the mixed precursor hydrogels were successfully fitted with eq 1 (Supporting Information Figures S5–S9), with the best-fit parameters describing the network characteristics ($\xi$ and $\Xi$) plotted as a function of temperature in Figure 7A,B.

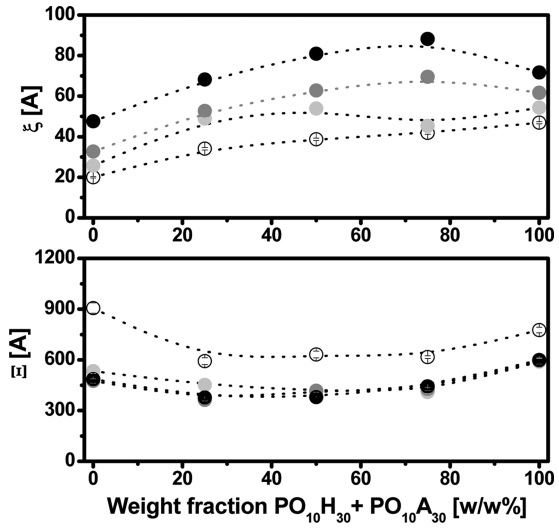


**Figure 7.** Correlation length ($\xi$) and the characteristic size of inhomogeneities ($\Xi$) as a function of the hydrogel composition at 22 °C (open circle), 32 °C (light gray circle), 37 °C (gray circle), and 45 °C (black circle).

From the results in Figure 6, it can be concluded that there is a clear effect of the measurement temperature on the nanostructure of the hydrogel. Similar to the $PO_{10}$ and $PO_{100}$ hydrogels, the increased measurement temperature increases the fluidity of the network (i.e., the ability of the network to self-diffuse), which results in an increase in $\xi$ and a decrease in $\Xi$ (Figure 7A,B). Despite the slower gelation kinetics and more homogeneous hydrogel network (concluded from the $I(q)$ results in Figure 4C) of $PO_{100}$, the mesh size of the $PO_{100}$ hydrogel is smaller than that of the $PO_{10}$ hydrogel. Furthermore, the results in Figure 7 show that the composition of the mixed precursor polymers used to prepare the hydrogel has a significant effect on the nanostructure of the hydrogel; as the temperature increases from 22 to 45 °C, the $\xi$ of the mixed PO(75/25), PO(50/50), and PO(25/75) hydrogel networks show larger values for $\xi$ and smaller values for $\Xi$ relative to what would be predicted based on a simple linear combination of $PO_{10}$ and $PO_{100}$ single precursor gel results. This result suggests that these mixed precursor hydrogels have higher heterogeneity than the single precursor hydrogels. In addition, given that the hydrogel indicators for heterogeneity deviate more significantly from the linear arithmetic average of the parameters for the two single precursor hydrogels as the temperature is increased, phase separation between the $PO_{10}$ precursors and the $PO_{100}$ precursors is likely to have occurred within the mixed precursor hydrogels, with the relative scattering intensities of these two domains changing differently as a function of temperature due to the different LCSTs of the polymer precursors.

**SANS of Single Precursor POEGMA Hydrogels with Different LCSTs.** The neutron scattering intensity, $I(q)$, as a function of the scattering vector ($q$) was also measured for the $PO_{10}H_{30}$ + $PO_{100}A_{30}$ and $PO_{100}H_{30}$ + $PO_{10}A_{30}$ hydrogels at 22 °C to compare the internal morphologies of these single precursor, different LCST gels relative to the single precursor, same LCST hydrogels which were also transparent (Figure 8 and Supporting Information Figure S9).

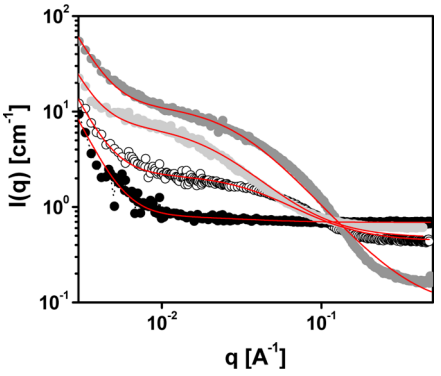


**Figure 8.** Scattering intensity at 22 °C of the single precursor hydrogels based on precursors with similar LCSTs (open circle) $PO_{100}H_{30}$ + $PO_{100}A_{30}$ and (light gray circle) $PO_{10}H_{30}$ + $PO_{10}A_{30}$ and precursors with different LCSTs (black circle) $PO_{10}H_{30}$ + $PO_{100}A_{30}$ and (gray circle) $PO_{100}H_{30}$ + $PO_{10}A_{30}$. The Ornstein–Zernike (OZ)–squared Lorentzian (SL) fits of the scattering intensities are shown as the red solid lines.

Compared to the neutron scattering intensity of the $PO_{10}$ and $PO_{100}$ hydrogels at low $q$ ($q \leq 10^{-2}$ Å) the hydrogel prepared from $PO_{10}H_{30}$ + $PO_{100}A_{30}$ scatters more (i.e., more inhomogeneous), whereas the hydrogel prepared from $PO_{100}H_{30}$ + $PO_{10}A_{30}$ scatters less (i.e., more homogeneous) (Figure 8). The difference in gelation kinetics ($PO_{10}H_{30}$ and $PO_{100}A_{30}$ cross-link in 20 s, whereas $PO_{100}H_{30}$ and $PO_{10}A_{30}$ cross-link in 230 s), coupled with the SANS results in Figure 8, could suggest that the presence of the $PO_{10}H_{30}$ precursor results in fast gelation and consequently more heterogeneous hydrogels. Given that these hydrogels remain transparent, the SANS result implies that while the different LCSTs of the precursors drives a phase separation upon gelation, the magnitude of that phase separation is limited by the covalent cross-link formation occurring between the two precursors on the time scale of phase separation; as such, the size of domains formed is likely limited due to network stiffness and the hydrogels remain transparent. Interestingly, recent work by Saffer and co-workers[30,31] have shown similar results for thionorbornene cross-linked PEG hydrogels prepared with short PEG chain lengths (4K and 8K g $mol^{-1}$), in which the short PEG chain length could not sufficiently counteract the hydrophobic effect of the norbornene end groups and


dx.doi.org/10.1021/ma5011827 | Macromolecules 2014, 47, 6017–6027

heterogeneous hydrogels were produced. While we cannot definitively rule this phenomenon out as a possible explanation for the hydrogel opacities observed, the fact that hydrogels prepared with the exact same total OEGMA monomer balance (i.e., same overall end-group composition and same overall hydrophilic/hydrophobic balance) can be made transparent (if only 2 precursors of different LCSTs are used) or highly opaque (if 4 precursors, 2 of each LCST value, are used) suggests to us that microphase separation is the more likely explanation. The absence of any sort of highly hydrophobic entity such as the norbornene group in our hydrogels further supports our hypothesis.

**Light Scattering of Single and Mixed Precursor POEGMA Hydrogels.** One homogeneous precursor ($PO_{100}$, transparent, Figure 1D) and one heterogeneous precursor (PO(50/50), opaque, Figure 1H) POEGMA hydrogel were characterized by light scattering (LS). The intensity profile was plotted with respect to the scattering vector $q$ following Bragg's law (eq 4)

$$q = \frac{4\pi \sin\left(\frac{2\theta}{2}\right)}{\lambda} \tag{4}$$

where the real space distance is calculated by $d = 2\pi/q$. The intensity profiles (corrected for the scattering from the cuvette) for $PO_{100}$ and PO(50/50) are shown in Figure 9. The signal was fitted using Gaussian distributions. Structural peaks at $d$ = 2.9 $\mu$m ($Q = \pm 2.19 \times 10^{-4}$ Å$^{-1}$) were observed in the optically transparent $PO_{100}$ hydrogel together with a central peak indicative of longer length scales which cannot be resolved by the light scattering technique. For the opaque PO(50/50) hydrogel, a similar length scale of structural peak at $d$ = 2.2 $\mu$m ($Q = \pm 2.84 \times 10^{-4}$ Å$^{-1}$) was observed but at significantly lower intensity than those observed for $PO_{100}$. As such, scattering in PO(50/50) was mainly due to the central peak (i.e., due to larger features that cannot be resolved by LS). From the half-width at half-maximum of the central peak of $7.02 \times 10^{-5}$ Å$^{-1}$, a lower bound for the size of the observed structures in the opaque PO(50/50) hydrogel can be estimated to be approximately 8 $\mu$m, although structures significantly larger are also likely to also be present. No additional peaks were observed at higher scattering angles, which excludes the possibility of the presence of structures of smaller length scales (i.e., >1 $\mu$m). The data thus suggest that the scattering length scales in the opaque hydrogel samples are significantly longer than the transparent hydrogel sample.

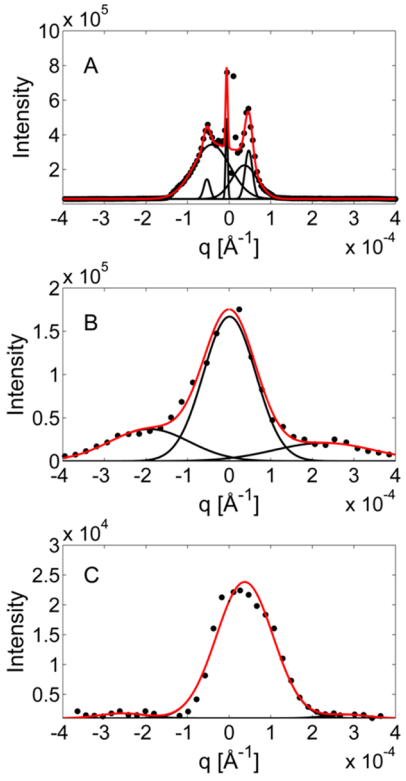


**Figure 9.** Light scattering intensity as measured for (A) the cuvette (= background), (B) the single precursor POEGMA hydrogel $PO_{100}$, and (C) the mixed precursor POEGMA hydrogel PO(50/50).

## DISCUSSION

The scattering intensity functions of the $PO_{10}$ and $PO_{100}$ single precursor hydrogels shown in Figure 4A,B can be represented by a summation of dynamic (OZ) and static (SL) fluctuations, typically used for the characterization of hydrogel systems;[7,24] in contrast, the scattering intensity function of the $PO_0$ hydrogel could be fully fit by considering static (SL) fluctuations only. Consequently, it can be concluded that the $PO_{10}$ and the $PO_{100}$ hydrogels are more homogeneous and contain less "frozen" domains than the $PO_0$ hydrogel. This result is consistent with the observed opacity, the faster rate of gelation (limiting the potential degree of diffusional mixing of the two reactive precursor polymers), and the significantly lower phase transition temperature (facilitating temperature-induced phase separation into domains) of $PO_0$ relative to the other hydrogels assessed. In contrast, slower gelation kinetics and lower cross-link densities result in more homogeneous hydrogels that show a mesh size of 2−7 nm (depending on temperature) with inhomogeneities on a size range of 40−60 nm (i.e., inhomogeneities are present, but on a length scale that the optical transparency of the hydrogels is not affected) for the transparent $PO_{10}$ and the $PO_{100}$ hydrogels.

For the $PO_{10}$ and $PO_{100}$ hydrogels, temperature has a clear impact on the hydrogel mesh size ($\xi$) and the size of inhomogeneities ($\Xi$) observed within those hydrogel networks (Figure 5A,B). For both hydrogels, the mesh size increases with increasing temperature. Although this result is counterintuitive when compared to the macroscopic behavior of thermoresponsive hydrogels when heated to a temperature ($T$) close to the critical phase transition temperature ($T_c$) (i.e., hydrogel deswelling would be expected to reduce the mesh size), an increase in $\xi$ has been similarly observed for thermoresponsive poly(*N*-isopropylacrylamide) (PNIPAAm) and dimethylacrylamide (DMAAm) hydrogels.[23,24] The increase in $\xi$ seems to diverge asymptotically as $T - T_c$ approaches 0, which has also been shown by Shibayama for conventional free radical-polymerized PNIPAAm hydrogels (and in fact holds true for any phase transition in materials).[23,24] As the temperature increases, the fluidity (i.e., self-diffusion) of the polymer chains in the network increases, leading to increased dynamic fluctuations and consequently a larger $\xi$. As the network collapses at $T_c$, this fluidity is lost, and the hydrogel network can be described by static fluctuations only (as was observed experimentally for the $PO_0$ hydrogel, Figure 4A). It was expected based on the measured macroscopic phase transition of $PO_{10}$ that $\xi$ would diverge (i.e., approach infinity) around the VPTT of 32−33 °C; however, this was not observed


dx.doi.org/10.1021/ma5011827 | Macromolecules 2014, 47, 6017−6027

experimentally. Furthermore, the relatively small but still significant decrease in Ξ as observed here for the $PO_{10}$ and $PO_{100}$ hydrogels is generally not observed for conventional thermoresponsive PNIPAAm hydrogels, for which Ξ remained relatively constant over the whole temperature range probed. We hypothesize that this difference is related not to the different gelation mechanisms but rather to the fundamental chemical differences between PNIPAAm and POEGMA. The phase transition in PNIPAAm polymers is characterized by a transition from hydrogen bonding with water at $T$ < LCST to intramolecular hydrogen bonding between the amide nitrogen and the amide carbonyl group at $T$ > LCST.[32] As POEGMA polymers lack a hydrogen bond donor, the phase transition in POEGMA hydrogels is instead characterized by continuous dehydration followed by chain aggregation. On this basis, we expect that the observed decrease in Ξ (related to the size of the inhomogeneous domains) is related to a collapse of these domains (40−60 nm in size) due to continuous dehydration at higher temperatures.

Contrary to the single precursor hydrogels, the mixed precursor hydrogels all appear translucent (Figure 1). The gelation experiments (Figure 3B) showed that this translucency did not originate from a volume phase transition but rather was induced during macroscopic gelation of the precursors (indeed, at times well before macroscopic gelation was observed). This suggests that opacity of the mixed PO(75/25), PO(50/50), and PO(25/75) hydrogels is due to the presence of larger inhomogeneities in the hydrogel network. SANS scattering intensity functions of these mixed precursor hydrogels could be successfully described by a combination of dynamic (OZ) and static (SL) fluctuations. As the hydrogel composition shifts from exclusively $PO_{100}$ precursors to exclusively $PO_{10}$ precursor, it can be expected that the cross-link density increases, which increases scattering (as observed). Similar results were obtained for PNIPAAm hydrogels cross-linked with $N'N$-methylenebis(acrylamide) (MBAAm), in which $I(q)$ increased with increasing mole fraction of MBAAm.[33] A difference in the network structure was also observed, as the mixed precursor hydrogels generally show larger mesh sizes and (surprisingly, given the opacity) smaller inhomogeneities than the single precursor hydrogels (Figure 7A,B). We anticipate that the larger domains that led to hydrogel opacity were at a larger length scale than could be probed by SANS (i.e., inhomogeneities occur at multiple length scales in these hydrogels). Consequently, complementary LS experiments were performed on one transparent single precursor hydrogel ($PO_{100}$) and one mixed precursor hydrogel (PO(50/50), the hydrogel with the fastest development of opacity upon gelation). The scattering intensity functions showed a clear shift from structures predominantly around 2.9 μm for the $PO_{100}$ hydrogel to structures that are significantly larger (>8 μm) for the PO(50/50) hydrogel (Figure 9). These results strongly suggest that the mixed precursor hydrogels contain significant concentrations of very large domains that cause scattering and thus impart an opaque appearance of these hydrogels.

From an application point of view, the knowledge gained through this study regarding the internal morphology of injectable POEGMA hydrogels provides significant insight into the design of such hydrogels for targeted applications. For example, hydrogels designed for ophthalmic applications (i.e., vitreous humor substitutes or prolonged drug delivery vehicles to the back of the eye) must be designed to strike a balance between the cross-link density (which determines $G'$ and, in our case, the degradation rate[12]) and the optical transparency. High cross-link densities can be achieved (using $PO_0$ precursors), but at the expense of optical clarity of the hydrogel. Conversely, highly transparent $PO_{100}$ hydrogels can be prepared, but the mechanical strength and degradation stability of those hydrogels are inherently limited. On the basis of the transparency of the hydrogel produced by mixing a one $PO_{10}$ precursor with one $PO_{100}$ precursor (one functionalized with hydrazides and the other with aldehydes, Figure 1), we anticipate that improved mechanics/degradation lifetimes while preserving transparency may be achievable by mixing precursors with different LCSTs. The difference in the network structure between the single and mixed precursor hydrogels also provides an interesting opportunity in terms of understanding and optimizing injectable POEGMA hydrogels for controlled release applications, given that drug release kinetics are directly governed by the internal morphology hydrogel network. A full evaluation of the macroscopic (physiochemical, biological, and drug release) properties of these mixed precursor POEGMA hydrogels in the context of biomedical applications will be discussed in a follow-up study.

## ■ CONCLUSIONS

Small-angle neutron scattering and light scattering have been applied to probe the internal morphology of injectable *in situ* gelling hydrogels based on hydrazide and aldehyde-functionalized POEGMA precursor polymers with varying lower critical solution temperatures. Transparent hydrogels are formed if two precursor polymers with similar or dissimilar LCST values were mixed, provided the LCST is not too low or the cross-linking potential of the precursors is not too high, although the internal homogeneity of the hydrogels prepared with different LCST precursors is significantly higher; in contrast, highly opaque hydrogels with very large inhomogeneous domains are formed if pairs of precursors with different LCST values are coextruded (i.e., in cases in which gelation can proceed even if phase separation occurs). Thus, by tuning the number and LCST values of polymer precursors used to prepare the injectable hydrogel, gel morphologies can be tuned over a broad range. This insight offers significant potential to rationally design POEGMA-based *in situ* gelling hydrogels for targeted biomedical applications, particularly in the context of controlled release of therapeutics with specific affinities to the inhomogeneous phase.

## ■ ASSOCIATED CONTENT

### Supporting Information

UV−vis gelation experiments and curve-fitted data for all measured SANS profiles. This material is available free of charge via the Internet at http://pubs.acs.org.

## ■ AUTHOR INFORMATION

### Corresponding Author

*E-mail hoaretr@mcmaster.ca (T.H.).

### Notes

The authors declare no competing financial interest.

## ■ ACKNOWLEDGMENTS

Funding from 20/20: NSERC Ophthalmic Materials Research Network, the Ontario Ministry of Research and Innovation Postdoctoral Fellowship program (N.M.B.S.), and NSERC

CREATE-IDEM (Integrated Design of Extracellular Matrices) (E.B.) is gratefully acknowledged. This research was also funded by the Natural Sciences and Engineering Research Council of Canada (NSERC), the National Research Council Canada (NRC), the Canada Foundation for Innovation (CFI), and the Ontario Ministry of Economic Development and Innovation. M.C.R. is the recipient of an Early Researcher Award of the Province of Ontario. This work utilized facilities supported in part by the National Science Foundation under Agreement DMR-0944772. We acknowledge the support of Dr. Boualem Hammouda and the National Institute of Standards and Technology, U.S. Department of Commerce, in providing the neutron research facilities used in this work.

## REFERENCES

(1) Langer, R.; Tirrell, D. A. *Nature* **2004**, *428*, 487−492.
(2) Slaughter, B. V.; Khurshid, S. S.; Fisher, O. Z.; Khademhosseini, A.; Peppas, N. A. *Adv. Mater.* **2009**, *21*, 3307−3329.
(3) Hoare, T.; Kohane, D. S. *Polymer* **2008**, *49*, 1993−2007.
(4) Hoffman, A. S. *Adv. Drug Delivery Rev.* **2002**, *54*, 3−12.
(5) Tibbitt, M. W.; Anseth, K. S. *Biotechnol. Bioeng.* **2009**, *103*, 655−663.
(6) Matsunaga, T.; Sakai, T.; Akagi, Y.; Chung, U.; Shibayama, M. *Macromolecules* **2009**, *42*, 1344−1351.
(7) Shibayama, M. *Macromol. Chem. Phys.* **1998**, *199*, 1−30.
(8) Metters, A. T.; Anseth, K. S.; Bowman, C. N. *J. Phys. Chem. B* **2001**, *105*, 8069−8076.
(9) Malkoch, M.; Vestberg, R.; Gupta, N.; Mespouille, L.; Dubois, P.; Mason, A. F.; Hedrick, J. L.; Liao, Q.; Frank, C. W.; Kingsbury, K.; Hawker, C. J. *Chem. Commun.* **2006**, 2774−2776.
(10) Patenaude, M.; Smeets, N. M. B.; Hoare, T. *Macromol. Rapid Commun.* **2014**, *35*, 598−617.
(11) Smeets, N. M. B.; Bakaic, E.; Patenaude, M.; Hoare, T. 2014.
(12) Smeets, N. M. B.; Bakaic, E.; Patenaude, M.; Hoare, T. *Chem. Commun.* **2014**, *50*, 3306−3309.
(13) Patenaude, M.; Hoare, T. *ACS Macro Lett.* **2012**, *1*, 409−413.
(14) Patenaude, M.; Hoare, T. *Biomacromolecules* **2012**, *13*, 369−378.
(15) Ito, T.; Yeo, Y.; Highley, C. B.; Bellas, E.; Kohane, D. S. *Biomaterials* **2007**, *28*, 3418−3426.
(16) Alves, M.; Young, C. *Biomed. Mater.* **2012**, *7*, 024106.
(17) Ossipov, D. A.; Hilborn, J. *Macromolecules* **2006**, *39*, 1709−1718.
(18) Oommen, O. P.; Wang, S.; Kisiel, M.; Sloff, M.; Hilborn, J.; Varghese, O. P. *Adv. Funct. Mater.* **2013**, *23*, 1273−1280.
(19) Hudson, S. P.; Langer, R.; Fink, G. R.; Kohane, D. S. *Biomaterials* **2010**, *31*, 1444−1452.
(20) Lee, K. Y.; Bouhadir, K. H.; Mooney, D. J. *Macromolecules* **2000**, *33*, 97−101.
(21) Lutz, J.-F. *J. Polym. Sci., Part A: Polym. Chem.* **2008**, *46*, 3459−3470.
(22) Lutz, J.-F.; Weichenhan, K.; Akdemir, Ö.; Hoth, A. *Macromolecules* **2007**, *40*, 2503−2508.
(23) Shibayama, M.; Morimoto, M.; Nomura, S. *Macromolecules* **1994**, *27*, 5060−5066.
(24) Shibayama, M.; Isono, K.; Okabe, S.; Karino, T.; Nagao, M. *Macromolecules* **2004**, *37*, 2909−2918.
(25) Ornstein, L. S.; Zernicke, F. *Proc. Acad. Sci. Amsterdam* **1914**, *17*, 793−806.
(26) Sivakumaran, D.; Maitland, D.; Hoare, T. *Biomacromolecules* **2011**, *12*, 4112−4120.
(27) Campbell, S. B.; Patenaude, M.; Hoare, T. *Biomacromolecules* **2013**, *14*, 644−653.
(28) Mallam, S.; Horkay, F.; Hecht, A. M.; Geissler, E. *Macromolecules* **1989**, *22*, 3356−3361.
(29) Shibayama, M.; Norisuye, T.; Nomura, S. *Macromolecules* **1996**, *29*, 8746−8750.
(30) Saffer, E. M.; Lackey, M. A.; Griffin, D. M.; Kishore, S.; Tew, G. N.; Bhatia, S. R. *Soft Matter* **2014**, *10*, 1905−1916.
(31) Cui, J.; Lackey, M. A.; Madkour, A. E.; Saffer, E. M.; Griffin, D. M.; Bhatia, S. R.; Crosby, A. J.; Tew, G. N. *Biomacromolecules* **2012**, *13*, 584−588.
(32) Sun, S.; Wu, P. *Macromolecules* **2013**, *46*, 236−246.
(33) Takata, S.; Norisuye, T.; Shibayama, M. *Macromolecules* **2002**, *35*, 4779−4784.